Published in final edited form as:
J Magn Reson. 2011 October ; 212(2): 370–377. doi:10.1016/j.jmr.2011.07.018.

Relaxation Times and Line Widths of Isotopically-Substituted Nitroxides in Aqueous Solution at X-band

Joshua R. Biller[a,b], **Virginia Meyer**[a,b], **Hanan Elajaili**[a,b], **Gerald M. Rosen**[b,c,d], **Joseph P.Y. Kao**[b,c,e], **Sandra S. Eaton**[a,b], and **Gareth R. Eatona**[a,b]

[a]Department of Chemistry and Biochemistry, University of Denver, Denver, CO 80208

[b]Center for EPR Imaging in Vivo Physiology, University of Denver, Denver, CO 80208 and University of Maryland, Baltimore, Baltimore, MD, 21201

[c]Center for Biomedical Engineering and Technology, University of Maryland, Baltimore, Baltimore, MD, 21201

[d]Department of Pharmaceutical Sciences, University of Maryland, Baltimore, Baltimore, MD, 21201

[e]Department of Physiology, University of Maryland, Baltimore, Baltimore, MD, 21201

Abstract

Optimization of nitroxides as probes for EPR imaging requires detailed understanding of spectral properties. Spin lattice relaxation times, spin packet line widths, nuclear hyperfine splitting, and overall lineshapes were characterized for six low molecular weight nitroxides in dilute deoxygenated aqueous solution at X-band. The nitroxides included 6-member, unsaturated 5-member, or saturated 5-member rings, most of which were isotopically labeled. The spectra are near the fast tumbling limit with $T_1 \sim T_2$ in the range of 0.50 to 1.1 μs at ambient temperature. Both spin-lattice relaxation T_1 and spin-spin relaxation T_2 are longer for ^{15}N- than for ^{14}N-nitroxides. The dominant contributions to T_1 are modulation of nitrogen hyperfine anisotropy and spin rotation. Dependence of T_1 on nitrogen nuclear spin state m_I was observed for both ^{14}N and ^{15}N. Unresolved hydrogen/deuterium hyperfine couplings dominate overall line widths. Lineshapes were simulated by including all nuclear hyperfine couplings and spin packet line widths that agreed with values obtained by electron spin echo. Line widths and relaxation times are predicted to be about the same at 250 MHz as at X-band.

1. INTRODUCTION

Optimization of nitroxides as probes for *in vivo* EPR imaging requires understanding of multiple factors that contribute to improved signal-to-noise (S/N). The goal of the present study is to define for nitroxides (a) the features of the molecules that impact the inherent relaxation-determined spin packet line widths, (b) the relaxation mechanisms that dominate spin lattice relaxation, and (c) the structural features that determine the unresolved hyperfine

Corresponding author: Sandra S. Eaton, Department of Chemistry and Biochemistry, University of Denver, Denver, CO 80208, seaton@du.edu, ph: 303-871-3102, fax: 303-871-2254.

splittings. These studies reveal patterns that guide the design and selection of nitroxides for imaging experiments.

For low molecular weight nitroxides in water, EPR spectra at X-band and lower frequencies are near the rapid tumbling limit: tumbling correlation times (τ) are of the order of 10 ps, $T_1 \sim T_2$, saturation recovery curves can be fit with a single exponential, and line widths and T_2 are weakly dependent on frequency because the dominant anisotropic interaction is the frequency-independent nuclear hyperfine. Recent work on the frequency dependence of T_1 for nitroxides has focused on the slower tumbling regime with τ values in the range of 10^{-9} to 10^{-10} s [1-3] where T_1 is dependent on frequency below X-band (9 GHz). However, in the fast tumbling regime T_1 for nitroxides is predicted to be independent of frequency below X-band [4]. Thus, although the ultimate goal is imaging at frequencies in the 250 MHz to 1 GHz range, advantage was taken of the higher signal-to-noise (S/N) achievable with smaller sample size at X-band to explore concentration and structure dependence of relaxation times and line widths.

The study included nitroxides with 6-member (**1**), unsaturated 5-member (**2**), or saturated 5-member (**3**) rings (Fig. 1). Each was studied with both ^{14}N and ^{15}N isotopes. Since substitution of ^{1}H by ^{2}H substantially narrows the EPR signal and improves S/N, the study focused on deuterium-substituted nitroxides. Nitroxide **2** was selected for study because the unique ring hydrogen has been shown to have a hyperfine splitting that is a convenient monitor of oxygen concentration [5]. The low concentration, continuous wave (CW) line widths, spin-packet line widths required for simulations including all nuclear hyperfine splittings, and directly-measured relaxation T_1 and T_2 were compared.

2. EXPERIMENTAL

2.1 Preparation of nitroxides

1a and **1b** with > 98% isotope purity were purchased from CDN Isotopes (Quebec, Canada). A second sample of **1a** was prepared as described in the following paragraphs. **2a** and **2b** were prepared as previously reported [5] and provided by Prof. Halpern (University of Chicago). The syntheses of **3a** and **3b** were reported previously [6].

4-Oxo-2,2,6,6-tetra($^{2}H_3$)methyl-(3,3,5,5-$^{2}H_4$,1-^{14}N)piperidine [4]—This compound was prepared following the general procedure of Lin *et al*. [7] with minor modifications. In a dry box with a positive N_2 flow, $^{14}N^{2}H_4Cl$ (Cambridge Isotopes, 98% 3.45 g, 60 mmol) was added to a 250-mL round bottom flask, which contained oven-dried anhydrous Na_2CO_3 (3.18 g, 30 mmol) and oven-dried MgO (3.0 g, 75 mmol). After the addition was complete, acetone-d_6 (12.5 mL, 150 mmol; 99.9%) was introduced into the flask via a canula under N_2 pressure. The flask was capped with a rubber septum, heated for 3 days in an oil bath at 50°C, and then allowed to cool. Then, acetone-d_6 (20 mL) was added to the flask and the resulting mixture was filtered. The filter cake was crushed into a fine powder, washed with dry ether and acetone-d_6 (1:1 mixture, 20 mL) and again filtered; this procedure was repeated three more times. The combined filtrates were concentrated on a rotary evaporator to give a red liquid (6.0 g), a portion of which was distilled to yield a yellow liquid (bp 60-64°C at 12 mm Hg) [7], which solidified upon cooling. Distillation of **4** did not significantly affect the yield of **1a**; therefore, crude **4** was used for the next reaction without further purification.

4-Oxo-2,2,6,6-tetra($^{2}H_3$)methyl-1-(3,3,5,5-$^{2}H_4$,1-^{14}N)piperidinyloxyl [1a]—To a solution of crude 4-oxo-2,2,6,6-tetra($^{2}H_3$)methyl-(1,3,3,5,5-$^{2}H_5$,1-^{14}N)piperidine [**4**] (6.0 g, 35.3 mmol) dissolved in D_2O (60 mL), was added oven-dried Na_4EDTA (0.55 g, 1.5 mmol) and oven-dried Na_2WO_4 (0.55 g, 1.7 mmol). Upon dissolution of the salts, H_2O_2 (30% in

H_2O, 6 mL) was added and the reaction was allowed to proceed in the dark for 8-10 days. The reaction mixture was filtered and extracted with ether (3 × 50 mL). The ether solution was first washed with cold dilute ^2HCl (10% in D_2O, 2 × 20 mL) and then a saturated solution of Na_2CO_3 in D_2O (10 mL). The remaining ether solution was dried over anhydrous $MgSO_4$, and then evaporated to dryness. This nitroxide was chromatographed using silica gel, eluting with hexane:ether (2:1) to afford 4-oxo-2,2,6,6-tetra($^2H_3$)methyl-1-(3,3,5,5-$^2H_4$,1-^{14}N)piperidinyloxyl **1a**, as a red oil, which solidified in the cold (3.1 g, 48% yield). IR ($CHCl_3$): 1720 cm^{-1} (C=O). Anal. calculated for $C_9\ ^2H_{16}\ ^{14}NO_2$: C, 58.00; ^2H, 8.65; ^{14}N, 7.52. Found: C, 58.09; ^2H, 8.77; ^{14}N, 7.41. EPR spectra and relaxation times for this preparation of **1a** and for the sample of **1a** purchased from CDN isotopes were indistinguishable.

2.2 Preparation of solutions

Weighed samples of radicals were dissolved in water. Solutions in thin-wall 0.97 mm i.d. Teflon tubing were placed inside 4 mm o.d. quartz tubes. Gaseous N_2 was passed over the sample via a thin Teflon tube that extended to the bottom of the quartz sample tube. O_2 and N_2 exchange through the tubing. The purging was continued until no further change in line width or relaxation time was observed. Integrals of CW spectra were checked to ensure that water evaporation was small enough that it did not significantly change the solution concentrations.

2.3 Spectroscopy

Experiments were performed at room temperature, which was ca. 20-22 °C at the sample position in the resonator. X-band CW EPR spectra were obtained on a Bruker EMX-Plus spectrometer. Microwave power incident on the sample, magnetic field modulation amplitude, and modulation frequency were adjusted to ensure that the observed line widths were not broadened by experimental parameters. Reproducibility of oxygen removal was checked. The effectiveness of the deoxygenation methodology was verified with an Oxylab pO_2 fluorescent probe (Oxford Optronix, U.K.). Spectra of **1a**, **2a**, or **3b** in D_2O were essentially indistinguishable from those in H_2O. The slightly higher viscosity of D_2O than of H_2O causes proportional increases in tumbling correlation times that could be detected by changes in T_2 measured by spin echo. However, this change is T_2 is within the uncertainty in determination of T_2 by simulation of CW lineshapes.

T_2 relaxation times were measured by two-pulse electron spin echo on a Bruker E580 or on a locally-built pulsed spectrometer [8] with a Bruker ER4118-X5MS split ring resonator. Both spectrometers use nominal 1 kW TWT amplifiers. The time constant for spin echo dephasing is designated as T_m [9]. For a molecule tumbling rapidly in fluid solution $T_m = T_2$ so in this paper the spin echo dephasing time constant is designated as T_2. T_1 relaxation times were measured by inversion recovery on these two spectrometers, or by saturation recovery on the E580 with a Bruker ER4118-X5MS split ring resonator or a home-built spectrometer [10] using the 5-loop-4-gap resonator described in ref. [11]. Values of T_1 obtained by inversion recovery and saturation recovery for selected samples were compared and found to be in good agreement, within experimental uncertainty. Inversion recovery inherently provides higher S/N, so that is the method of choice for T_1 measurements of nitroxides in this fast motional regime. Values of T_1 obtained by inversion recovery are reported in the tables. Results obtained on different spectrometers with several operators were in good agreement.

2.4 Fitting of exponentials to pulse data and simulations of CW spectra

Two-pulse echo decays, inversion recovery curves, and saturation recovery curves fit well with a single exponential, using a least-squares criterion. Reported relaxation times are

averages of at least 3 replicates. CW EPR spectra were simulated using the shareware EasySpin 3.1.6 (http://www.easyspin.org/) and using locally-written Fortran programs, with guidance from published hyperfine values for **1a** [12], **2a** [12,13], and saturated 5-member ring nitroxides (pyrrolidines) similar to **3a** [14]. ^{2}H couplings were calculated from literature values of ^{1}H couplings using the ratio $\gamma_D/\gamma_H = 0.153$. Hyperfine couplings are sensitive to solvent [13], so small differences from previously reported values were allowed in the simulations. Spin packet line widths calculated from T_2 were substituted into the Kivelson equation [15] for the dependence of line width on nuclear spin, $\Delta B = A + B\, m_I + C\, m_I^{\,2}$ [16]. Equations presented in Chasteen and Hanna were used to calculate the molecular tumbling correlation time τ from the value of B [17]. Since ^{14}N A = 16.1 to 16.4 G for **1, 2**, and **3** in water at 20° C, it was assumed that the anisotropic g and A_N values also would be similar for the three nitroxides. Based on literature reports the following parameters were used in analyzing the tumbling correlation times: $g_x = 2.0092$, $g_y = 2.0061$, $g_z = 2.0022$. $A_x = 5.5$, $A_y = 6.3$, and $A_z = 35.9$ G for ^{14}N [18,19]. Average values of τ based on CW spectra for ^{14}N and ^{15}N analogs at three concentrations are 9, 13, and 19 ps for **1, 2**, and **3**, respectively. To fit these τ values to the Stokes-Einstein equation ($\tau = c_{slip}\, V\, \eta/kT$, V = molecular volume, k = Boltzmann's constant) required c_{slip} of 0.11, 0.15, and 0.21 for **1, 2**, and **3**, respectively. The value of c_{slip} for **1** is similar to the previously reported values of 0.12 in 1:1 water glycerol [20] and 0.13 in glycerol [18]. Trends in the values of c_{slip} are consistent with the expectation of increasing solute-solvent interaction for ketone < amide < acid.

3. RESULTS

3.1 Spin-spin and spin-lattice relaxation times

Directly-measured relaxation times for the six radicals in 0.25 mM aqueous solutions are summarized in Table 1 for the center-field lines of the ^{14}N nitroxides and the low-field lines of the ^{15}N nitroxides. For the ^{14}N-nitroxides T_2 for the low-field line is 2 to 5% longer than for the center line and T_2 for the high-field line is 25 to 60% shorter than for the center line. For the ^{15}N-nitroxides T_2 for the high-field lines is 25 to 60% shorter than for the low-field lines. The modest dependence of T_2 on m_I and similarity in values of T_1 and T_2 (Table 1) are consistent with the fast tumbling regime. For comparison with simulations of CW spectra, T_2 was converted to peak-to-peak spin packet line widths, ΔB_{sp}, using the relationship for a Lorentzian line, Eq. (1):

$$\Delta B_{sp}(G) = \frac{2}{\sqrt{3}\gamma T_2} = \frac{6.56 \times 10^{-8}\,\text{G s}}{T_2(\text{s})} \qquad (1)$$

The much larger overall line widths, ΔB_{pp}, than spin packet line widths ΔB_{sp} (Table 1) reflect the substantial contributions from hydrogen/deuterium hyperfine splittings.

3.2 Contributions to T_1

Values of T_1 in 0.25 mM aqueous solutions (Table 1) are in good agreement with a report at X-band for 0.5 mM solutions at 20°C: $T_1 = 0.49$ μs for **1a** and $T_1 = 0.68$ μs for **2a** [2]. Although a dependence of T_1 on m_I was observed in the present study, recent models for nitroxide spin lattice relaxation do not include an m_I dependence [3,4,9,16,20-22]. The contributions to T_1 were therefore analyzed first for the average values observed for the 3 (or 2) values of m_I as summarized in Table 2 for 0.030 mM solutions. The m_I dependence is discussed separately in section 3.2.2. At these low concentrations the Heisenberg exchange contributions to the measured T_1 are negligible.

Spin-lattice relaxation for nitroxides in fluid solution has been analyzed in terms of contributions from spin rotation (Eq. (2)), modulation of g and A anisotropy by molecular tumbling, and generalized spin diffusion [3,4,9,16,20-22]. For nitroxides tumbling rapidly in deoxygenated fluid solution, spin rotation (Eq. (2)) makes a larger contribution to T_1 than in slower tumbling regimes [4,20], but as shown in Table 2 spin rotation alone is not sufficient to fully account for the relaxation times. Generalized spin diffusion (GSD) includes contributions from methyl rotation and modulation of intermolecular and intramolecular dipolar spin-spin interaction [4]. Other than the impact of slowing tumbling due to increased viscosity substitution of H_2O by D_2O did not change the relaxation times, which indicates that the intermolecular contribution to GSD is not significant for these experiments. With the exception of **3a** and one hydrogen in **2**, the nitroxides selected for study are perdeuterated, so intramolecular contributions from GSD are much smaller than for natural isotope abundance. Therefore GSD was not included in the calculations of T_1. At X-band (and lower frequencies) the contribution from modulation of g anisotropy is more than an order of magnitude smaller than from modulation of A anisotropy [4,20,22] (Eq. (3)) so inclusion of g anisotropy with an expression analogous to Eq. (3) had negligible impact on calculated T_1.

$$\frac{1}{T_1^{SR}}=\frac{\sum_{i=1}^{3}(g_i-g_e)^2}{9\tau} \tag{2}$$

where i = x,y,z and g_e is 2.0023.

3.2.1 Modulation of anisotropic nuclear hyperfine by tumbling—In recent papers the modulation of anisotropic nuclear hyperfine by tumbling has been described by Eq. (3), and called the END mechanism [4,22].

$$\frac{1}{T_1^{A}}=\frac{2}{9}I(I+1)\sum_i(A_i-\bar{A})^2J(\omega) \tag{3}$$

where A_i is a component of the nitrogen nuclear hyperfine in angular frequency units, $\bar{A}$ is the average nitrogen hyperfine, I is the nitrogen nuclear spin, and J(ω) is the spectral density function. Experimental values of T_1 (Tables 1 and 2) are systematically longer for nitroxides with ^{15}N than with ^{14}N, which is consistent with prior results [1,20,23]. The isotope effect arises from differences in both magnetic moment and nuclear spin I. ^{15}N has a larger magnetic moment than ^{14}N (μ_{14N}/μ_{15N} = 0.71) which increases A_i, but the I(I+1) term offsets this difference, so the ratio of the $^{14}N/^{15}N$ coefficients in Eq. (3) is $(0.71)^2 \times I_{14N}(I_{14N}+1)/ I_{15N}(I_{15N}+1)$ = 1.4. Thus, if modulation of anisotropic nitrogen hyperfine were the only contribution to T_1, T_1 for a ^{15}N-containing nitroxide would be 1.4 times larger than for the analogous ^{14}N-nitroxide. The $T_1(^{15}N)/ T_1(^{14}N)$ ratios in Table 2 are about 1.2, which is consistent with modulation of nitrogen hyperfine anisotropy, in addition to spin rotation that is independent of nitrogen hyperfine.

When motion is isotropic, the Bloembergen Pound Purcell (BPP) spectral density function, Eq. (4) is frequently used [3,22].

$$J_{BPP}(\omega)=\frac{\tau}{1+(\omega\tau)^2} \tag{4}$$

Calculations of T_1 using the experimentally determined values of the tumbling correlation time τ and Eq. (2) - (4) gave values in reasonable agreement with the experimental data (Table 2).

However, prior work on nitroxide relaxation has raised questions about the suitability of the BPP spectral density function. In studies of the temperature dependence of line widths of peroxylamine disulfonate (Fremy's salt) in glycerol:water mixtures [24], tumbling correlation times for **1a** in deuterated solvents [18], and T_1 for **1a** in toluene-d_8 [25] it was observed that the BPP spectral density function (Eq. 4) did not adequately model the data and that better agreement could be obtained by adding a parameter ε~ 4 as the coefficient of the $(\omega\tau)^2$ term. The Cole-Davidson spectral density function (Eq. 5) was developed in studies of dielectric relaxation [26] and has been applied to NMR as well as dielectric relaxation [27-29].

$$J_{CD}(\omega)=\frac{1}{\omega}\frac{\sin(\beta\cdot\arctan(\omega\tau))}{(1+(\omega\tau)^2)^{\beta/2}} \quad (5)$$

where β characterizes the distribution of correlation times. The smaller the value of β, the wider the distribution. For β = 1, $J_{CD}(\omega)$ reduces to $J_{BPP}(\omega)$. An EPR study of the temperature dependence of line widths for **1a** in toluene at L-band to X-band used a Cole-Davidson spectral density function with β = 0.83 [30]. In a study of nitroxide T_1 over a wide range of tumbling correlation times it was found that the Cole-Davidson spectral density function (Eq. 5) provided a better fit with experimental data than did the BPP model. The values of β ranged from 0.37 in o-terphenyl to 0.67 in 1:1 water:glycerol [20].

Calculation of T_1 including spin rotation (Eq. 2) and modulation of hyperfine anisotropy using Eq. (3) and (5) with β = 0.90 gave improved fit to the experimental data for **1, 2**, and **3** (Table 2).

3.2.2 Dependence of T_1 on nitrogen m_I—A dependence of T_1 on nitrogen m_I was observed (Table 3) with T_1 decreasing in the order low field > center field > high field. Although the differences are small, they were reproducible and many replicate measurements gave values of the ratios that are significantly different from 1. In an early variable temperature study of nitroxides in sec-butyl benzene a dependence of T_1 on m_I was observed, with magnitude comparable to experimental uncertainties [23] A dependence of T_1 on m_I was not observed in more recent studies of nitroxides in viscous solutions [20,22], but differences of the order of 10% are comparable to estimated uncertainties. A combination of ELDOR and saturation data for **1a** in toluene between 188 and 233 K (τ = 11.8×10^{-11} to 1.5×10^{-11} s) found ratios of T_1 for the low-field and high-field lines between about 1.1 and 1.25 (read from graph) [31], which indicates that the m_I dependence of T_1 (Table 3) persists at slower tumbling correlation times.

Early models for nitroxide spin lattice relaxation [15,24,32,33] included terms with m_I dependence as shown in Eq. 6.

$$\frac{1}{T_1^m}=[c_1\Delta A\,\Delta g\,\frac{\mu B}{\hbar}\,m_I+c_2(\Delta A)^2m_I^2]J(\omega) \quad (6)$$

where c_1 = -0.4 or -0.65, c_2 =0.033 or 0.05, $\Delta A = A_{zz} - 0.5(A_{xx}+A_{yy})$ with A in angular frequency units, and $\Delta g = g_{zz} - 0.5(g_{xx}+g_{yy})$.

We propose an empirical approach to modeling the m_I dependence of T_1. Since Eq. (3) for the END mechanism expresses the anisotropy differently than in eq. (6) we propose the expression for the m_I dependence shown in Eq. (7).

$$\frac{1}{T_1^m}=[c_1'\sum_i|(A_i-\bar{A})(g_i-\bar{g})|\frac{\mu B}{\hbar}m_I \quad (7)$$

The value of c_1' that gives the best fit to the combined experimental data for ^{14}N and ^{15}N nitroxides (Table 4) is -0.32 ± 0.03. The good agreement between the values of c_1' required to model the m_I dependence of T_1 for the ^{14}N and ^{15}N nitroxides confirms the linear dependence of the m_I term on nitrogen hyperfine anisotropy. For typical nitroxide g and A values, $\Delta A\ \Delta g$ is 1.5 times $\Sigma(g_i\text{-}g)(A_i\text{-}A)$ so $c_1' = -0.32$ makes the contribution from the m_I dependent term in eq. (7) smaller by a factor of 2 to 3 than that proposed in Eq. (6). Consistent with the predictions of Eq. (6), the experimental dependence of T_1 on m_I^2 is about an order of magnitude smaller than on m_I, which is too small an effect, relative to experimental uncertainty, to accurately define.

3.2.3 Concentration Dependence of T_1—The concentration dependence of T_1 (data not shown) is smaller than for T_2 (Table 5), which is discussed in the following paragraph. It has been shown previously that in the concentration range 0.57 to 53 mM T_2 for Fremy's salt was more dependent on concentration than was T_1 (factor of 20 vs. factor of 3.4), and the concentration effect on T_1 was attributed to Heisenberg exchange [34]. A spin lattice Heisenberg exchange relaxation process, which shortens T_1, can occur when two colliding radicals have different m_s. Since the populations of the two m_s states are approximately equal, only half of the collisions involve radicals with different m_s. The probability of Heisenberg exchange is smaller than the probability of colliding with a radical with different hyperfine interaction, which shortens T_2.

3.3 Spin-Spin Relaxation

The T_2 of 0.53 μs for **2a** (Table 1) is similar to values reported previously for aqueous solutions extrapolated to infinite dilution: 0.595 μs by electron spin echo at X-band and 0.47 μs by lineshape analysis at 250 MHz [35]. Near the rapid tumbling limit there are two contributions to T_2 – incomplete motional averaging of g and hyperfine anisotropy and spin-lattice relaxation, T_1. The similarity in T_1 and T_2 values in Table 1 indicates that T_1 makes a major contribution to T_2 and explains why T_2 is systematically longer for the ^{15}N- than for the ^{14}N- nitroxides.

The concentration dependence of T_2, was examined at four points between 0.02 and 0.30 mM, and the results are summarized in Table 5. The spin packet line widths extrapolated to infinite dilution are smaller (indicating longer T_2) for the ^{15}N-nitroxides than for the ^{14}N-nitroxides.

There is substantial variation in the concentration dependence of ΔB_{sp} (Table 5). The concentration dependence for **2a**, 160±10 mG/mM, agrees within experimental uncertainty with previous reports of 167 ± 3 mG [36] or 144 mG/mM [16]. The 170 ± 10 mG/mM concentration dependence for **2b** is similar to the previous report of 120 mG/mM [16]. The largest concentration dependence is observed for **2**. The large doublet hydrogen/deuterium hyperfine splitting (Table 6) for **2** results in a higher probability of collision with a radical in a different nuclear spin state. The concentration dependence is smallest for **3**, which is a carboxylic acid and is predominantly in its anionic form in neutral aqueous solution. The negative charge on **3** decreases the probability of collisions. The concentration dependence is slightly greater for ^{15}N than for ^{14}N. The smaller number of nitrogen nuclear spin states

increases the effective concentration in each line, but also decreases the probability of colliding with a radical in a different spin state.

3.4 CW lineshapes

As shown in Table 1 ΔB_{pp} is significantly larger than ΔB_{sp}, and within the set of nitroxides there are much larger variations in ΔB_{pp} than for ΔB_{sp}. Since decreasing ΔB_{pp} increases S/N, optimization of probes for in vivo imaging requires characterization of structural features that give rise to differences in hyperfine splittings. In addition, for EPR oximetry the parameter of interest is the change in ΔB_{sp} due to collision with molecular O_2. Thus it is important to confirm that simulations that include all hydrogen/deuterium hyperfine couplings give spin packet line widths that agree with values obtained directly by electron spin echo (Table 1).

CW spectra of the $m_I = 0$ lines for **1a, 2a, 3a** and the low-field line for **3b** are shown in Fig. 2. For each of the ring structures the low-field and center-field lines of ^{14}N- and low-field lines of ^{15}N-species have very similar line widths. The low field line of **3b** (Fig. 2D,F) is much sharper than the center field line of **3a** (Fig. 2C,E) because of the replacement of hydrogen by deuterium. The spectra of **3** shown in Fig. 2E,F were obtained in toluene, because the lower viscosity resulted in better resolution of the hydrogen hyperfine splitting (Fig. 2E) than was obtained in water. For each of the simulations the ΔB_{sp} used in the simulation is in good agreement with the value obtained by electron spin echo. The hyperfine couplings used in the simulations are shown in Table 6. For **1** and **2** simulation of the CW spectra for natural isotope abundance samples (spectra not shown) using values of the ^2H hyperfine couplings appropriately scaled to ^1H also were in good agreement with experiment.

A striking feature of the simulations, and a key factor in the small ΔB_{pp} for **1**, is the small coupling to the ring methyls. Substituents such as $-NH_2$ or $-OH$ (or derivatives of these) in the 4-position of a piperidine-1-oxyl, cause a conformation in which the bulky substituent is equatorial, and there is a large difference between the hyperfine couplings to two inequivalent sets of 6 hydrogens: equatorial ($a_H = 0.4$ to 0.5 G) and axial ($a_H \sim 0$ G) methyl groups [14,37], with resulting $\Delta B_{pp} > 1$ G [38]. If conformational dynamics are fast enough, the couplings to the axial and equatorial methyls are averaged and the twelve methyl hydrogens are equivalent on the EPR timescale. This is the case in the hydrogen-containing analog of **1** (average $a_H = 0.11$ G) [39] and in 2,2,6,6-tetramethyl-1-piperidinyloxyl (average $a_H = 0.22$ G). A double bond or two hydrogens at the 4-position appears to be required for the conformational averaging to be fast enough on the EPR timescale to give small averaged couplings to the methyls [38].

In 3-carbamoyl-2,2,5,5-tetramethyl-3-pyrrolin-1-yloxyl, CTPO, **5**, there are four inequivalent sets of 3 hydrogens, with almost equal couplings of about 0.2 G [5]. For **5** with normal isotopic abundance there is resolved hyperfine coupling to the methyl hydrogens and to the ring hydrogen [5]. The resolution of the hydrogen hyperfine splittings is sensitive to the O_2 concentration in solution. Complete deuteration of **5** results in hyperfine couplings that are too small to be resolved. The envelope of the unresolved deuterium couplings is a line that is broader than the resolved hydrogen hyperfine lines of **5**, and is less responsive to O_2 collisions. Deuteration of only the methyl groups of **5** produces **2** in which there is resolved splitting by the single ring hydrogen.

Simulations were performed initially of the spectra of **3a** in toluene, where there is partial resolution of the larger splittings (Fig. 2C), and then in water where the hyperfine splittings are not resolved (Fig. 2C). The overall lineshape is consistent with previously reported hyperfine splittings for this class of nitroxides [14], but uncertainties are greater than for **1** or

2. For **3** the asymmetric substitution of the ring and slow ring dynamics results in four inequivalent methyl groups with different hyperfine couplings, and a broad unresolved spectrum. When the hydrogen couplings were scaled to the values expected for deuterium the calculated lineshape was narrower than observed for **3b**. Simulations (Fig. 3d) indicate the presence of about 25% H (instead of D) for the unique ring H/D with large hyperfine coupling. Mass spectroscopy had shown essentially complete deuteration in **3b** [38]. However the EPR lineshapes are more sensitive than mass spectroscopy to incomplete deuteration at the unique site of the large hyperfine splitting.

3.5 Comparison with literature values for nitroxides

A summary of relaxation times for Fremy's salt reported T_1 = ca. 0.35 μs and T_2 = ca. 0.25 μs in air-saturated aqueous solutions at room temperature [37] and T_2 = 0.41 μs in degassed water [40]. Values of T_1 at X-band for low-molecular weight nitroxides in low viscosity solvents near 20° C [9] include **1a** in sec-butyl-benzene, 0.47 μs [23]; tempol in sec-butyl-benzene, 0.41 μs [23]; **1a** in toluene-d_8, 0.45 μs [25]; **1a** in water, 0.30 μs [41] and perdeuterated ^{15}N-tempol in water, 1μs (read from Fig 3 in [22]). The Freed group has performed extensive studies of the impact of molecular motion on lineshapes and T_2 [42,43]. These values are in the range of about 0.5 to 1 μs, consistent with the results reported here.

The spectrum of Fremy's salt does not have unresolved hyperfine coupling. The line width extrapolated to low concentration was 0.097 [44], which is similar to the 0.09 G values reported for nitroxides in Table 5. The Fremy's salt line width increases with concentration with a slope of 46 mG/mM between ~1 and 40 mM in aqueous 0.05 M K_2CO_3 (read from figure 3 of ref. [44]). The smaller concentration dependence of relaxation-determined line widths for Fremy's salt relative to neutral nitroxides such as **1** and **2** in water (Table 5) probably is due to the negative charges on the anion, analogous to observations on collision broadening of nitroxides by paramagnetic transition metal complexes [45,46]. The concentration dependence of T_2 and line width is expected to depend on charge surrounding the radical, spin distribution, overall size, solvent viscosity and pH. The trityl radicals used for *in vivo* imaging are larger than nitroxides and negatively charged [47], which makes relaxation less dependent on concentration than for neutral nitroxides such as **1** and **2**.

3.6 Predictions related to frequency dependence

In vivo EPR imaging experiments are performed at frequencies between about 250 MHz and 1.0 GHz [48]. The contributions to line widths from unresolved proton hyperfine are independent of frequency. At X-band and lower frequencies the anisotropy in nitrogen nuclear hyperfine dominates the terms that are averaged by tumbling and this contribution is independent of frequency, so the contributions to T_2 from incomplete motional averaging at 250 MHz to 1 GHz are predicted to be about the same as at X-band. At 250 MHz the values of T_2 for the low-field and center-field lines of **1a** obtained by rapid scan are 0.41 and 0.53 μs for 0.50 and 0.10 mM solutions, respectively [49]. These are similar to T_2 at X-band for the center-field line of **1a** of 0.59 and 0.68 μs for 0.25 mM and 0.030 mM solutions, respectively. In this rapid tumbling regime $T_1 \sim T_2$ so the experimental values of T_2 provide a lower limit on T_1 and requires that for **1a** T_1 at 250 MHz is ≥ 0.53 μs in 0.10 mM aqueous solution. Calculations of T_1 at 250 MHz including contributions from spin rotation (Eq. 2) and modulation of nitrogen nuclear hyperfine interaction described by Eq. (3) + (4), (3) + (5), or (3) + (5) + (7) predict T_1 for **1a** at 250 MHz of 0.66 to 0.78 μs in dilute aqueous solution. For **2a** and **3a** the longer tumbling correlation times predict somewhat shorter values of T_1 at 250 MHz and 1 GHz than at X-band but all of the models predict values of $T_1 \geq 0.5$ μs at 250 MHz. For nitroxide parameters the dependence of T_1 on m_I (Eq. 7) at 250 MHz is predicted to be smaller than that observed at X-band. Thus the results of the X-band relaxation time studies should also apply at lower frequencies.

4. CONCLUSIONS

The spin packet line widths in water (Table 1) are similar for the three ^{15}N-substituted radicals and somewhat narrower than for the ^{14}N-substituted analogs, due primarily to longer T_1 for ^{15}N than for ^{14}N. The negative charge on **3**, or a narrow line, such as for **1**, decreased the concentration dependence. The largest contribution to overall line width differences was from hydrogen (or deuterium) hyperfine splittings. As a result of the differences in hyperfine splittings, the CW peak-to-peak signal amplitude for **1a** is about 9 times greater than that for **5** and four times greater than for **2a**. Replacement of ^{14}N by ^{15}N improves signal amplitude by an additional factor of 1.5 due to the smaller number of hyperfine lines.

The spectra and relaxation times show that in aqueous solution at ambient temperature the six nitroxides studied are near the rapid tumbling limit and have $T_1 \sim T_2$. The dominant contributions to spin lattice relaxation are modulation of nitrogen hyperfine anisotropy and spin rotation. T_1 is less concentration dependent than T_2. Relaxation times and line widths for these nitroxides at 250 MHz in the rapid tumbling regime are predicted to be similar to values at X-band. Thus the results obtained at X-band provide the basis for selection and design of nitroxide probes for *in vivo* imaging at low frequencies.

Acknowledgments

This work was partially supported by NIH grants EB002807 and EB000557 to GRE and SSE, and P41 EB002034 to GMR and GRE; H. J. Halpern, PI. Discussion with James S. Hyde about the relative line widths of ^{14}N and ^{15}N nitroxides stimulated some of the measurements reported here. Compounds **2a** and **2b** were provided by Howard J. Halpern, University of Chicago. Velavan Kathirvelu, DU, assisted with preliminary measurements. We thank a reviewer for bringing ref. 31 to our attention.

References

1. Froncisz W, Camenisch TG, Ratke JJ, Anderson JR, Subczynski WK, Strangeway RA, Sidabras JW, Hyde JS. Saturation recovery EPR and ELDOR at W-band for spin labels. J Magn Reson. 2008; 193:297–304. [PubMed: 18547848]
2. Hyde JS, Yin J-J, Subczynski WK, Camenisch TG, Ratke JJ, Froncisz W. Spin-labeled EPR T_1 Values Using Saturation Recovery from 2 to 35 GHz. J Phys Chem B. 2004; 108:9524–9529.
3. Owenius R, Terry GE, Williams MJ, Eaton SS, Eaton GR. Frequency Dependence of Electron Spin Relaxation of Nitroxyl Radicals in Fluid Solution. J Phys Chem B. 2004; 108:9475–9481.
4. Mailer C, Nielsen RD, Robinson BH. Explanation of Spin-Lattice Relaxation Rates of Spin Labels Obtained with Multifrequency Saturation Recovery EPR. J Phys Chem A. 2005; 109:4049–4061. [PubMed: 16833727]
5. Halpern HJ, Peric M, Nguyen TD, Spencer DP, Teicher BA, Lin YJ, Bowman MK. Selective isotopic labeling of a nitroxide spin label to enhance sensitivity for T_2 oxymetry. J Magn Reson. 1990; 90:40–51.
6. Burks SR, Bakhshai J, Makowsky MA, Muralidharan S, Tsai P, Rosen GM, Kao JPY. ^{2}H,^{15}N-Substituted Nitroxides as Sensitive Probes for Electron Paramagnetic Resonance Imaging. J Org Chem. 2010; 75:6463–6467. [PubMed: 20828113]
7. Lin YJ, Teicher BA, Halpern HJ. Synthesis of 4-protio-3-carbamoyl-2,2,5,5-tetraperdeuteromethyl-3-pyrrolin-1-yloxy (mHCTPO): a selectively isotopically labeled compound for use in T_2 spin label oxymetry. J Labelled Compds Radiopharm. 1990; 28:621–31.
8. Quine RW, Eaton GR, Eaton SS. Pulsed EPR spectrometer. Rev Sci Instrum. 1987; 58:1709–23.
9. Eaton SS, Eaton GR. Relaxation times of organic radicals and transition metal ions. Biol Magn Reson. 2000; 19:29–154.
10. Quine RW, Eaton SS, Eaton GR. Saturation recovery electron paramagnetic resonance spectrometer. Rev Sci Instrum. 1992; 63:4251–62.

11. Rinard GA, Quine RW, Eaton SS, Eaton GR, Froncisz W. Relative benefits of overcoupled resonators vs. inherently low-Q resonators for pulsed magnetic resonance. J Magn Reson A. 1994; 108:71–81.
12. Gerson, F.; Huber, W. Electron Spin Resonance Spectroscopy of Organic Radicals. Wiley-VCH; Weinheim: 2003.
13. Bales BL, Blum RA, Mareno D, Peric M, Halpern HJ. Solvent and temperature dependence of the hyperfine coupling constants in CTPO. J Magn Reson. 1992; 98:299–307.
14. Rockenbauer A, Gyor M, Hankovszky HO, Hideg K. ESR of the conformation of 5- and 6-membered cyclic nitroxide (aminoxyl) radicals. Electron Spin Resonance. 1988; 11A:145–182.
15. Kivelson D. Theory of EPR [electron paramagnetic resonance] line widths of free radicals. J Chem Phys. 1960; 33:1094–1106.
16. Robinson BH, Mailer C, Reese AW. Linewidth analysis of spin labels in liquids. II. Experimental. J Magn Reson. 1999; 138:210–219. [PubMed: 10341124]
17. Chasteen ND, Hanna MW. Electron Paramagnetic Resonance Line Widths of Vanadyl (IV) α-hydroxycarboxylates. J Phys Chem. 1972; 76:3951–3958.
18. Hwang JS, Mason RP, Hwang L-P, Freed JH. Electron spin resonance studies of anisotropic rotational reorientation and slow tumbling in liquid and frozen media. III. Perdeuterated 2,2,6,6-tetramethyl-4-piperidone-N-oxide and an analysis of fluctuating torques. J Phys Chem. 1975; 79:489–511.
19. Labsky J, Pilar J, Lovy J. Magnetic resonance study of 4-amino -2,2,6,6-tetramethylpiperidine-N-oxyl and its deuterated derivatives. J Magn Reson. 1980; 37:515–522.
20. Sato H, Bottle SE, Blinco JP, Micallef AS, Eaton GR, Eaton SS. Electron spin-lattice relaxation of nitroxyl radicals in temperature ranges that span glassy solutions to low-viscosity liquids. J Magn Reson. 2008; 191:66–77. [PubMed: 18166493]
21. Robinson BH, Mailer C, Reese AW. Linewidth analysis of spin labels in liquids. I. Theory and data analysis. J Magn Reson. 1999; 138:199–209. [PubMed: 10341123]
22. Robinson BH, Haas DA, Mailer C. Molecular dynamics in liquids: spin-lattice relaxation of nitroxide spin labels. Science. 1994; 263:490–493. [PubMed: 8290958]
23. Percival PW, Hyde JS. Saturation-recovery measurements of the spin-lattice relaxation times of some nitroxides in solution. J Magn Reson. 1976; 23:249–257.
24. Goldman SA, Bruno GV, Freed JH. ESR Studies of anisotropic rotational reorientation and slow tumbling in liquid and frozen media. II. Saturation and nonsecular effects. J Chem Phys. 1973; 59:3071–3091.
25. Schwartz RN, Jones LL, Bowman MK. Electron spin echo studies of nitroxide free radicals in liquids. J Phys Chem. 1979; 83:3429–3439.
26. Davidson N, Cole RH. Dielectric relaxation in glycerol, propylene glycol, and n-propanol. J Chem Phys. 1951; 19:1484–1490.
27. Blochowicz T, Kudik A, Benkhof S, Senker J, Rossler E, Hinze G. The spectral density in simple organic glass formers: comparison of dielectric and spin-lattice relaxation. J Chem Phys. 1999; 110:12011–12022.
28. Friedrich A, Doelle A, Zeidler MD. Reorientational dynamics of glycerol derived from temperature-dependent multi-nuclear magnetic resonance relaxation data. Magn Reson Chem. 2003; 41:813–818.
29. Ueda T, Nakamura N. ^{1}H MAS NMR study of local structure and dynamics of water molecule in (+-)-[Co(en)$_3$] Cl$_3$-nD$_2$O. J Phys Chem B. 2003; 107:13681–13687.
30. Hwang JS, Al-Janavi YT. Frequency dependent study of the correlation functions in EPR spectroscopy - the Cole Davidson approach. 1. Perdeuterated 2,2,6,6-tetramethyl-4-piperidone N-oxide in toluene. Spect Chim Acta A. 2000; 56:273–284.
31. van der Drift E, Rousseeuw BAC, Smidt J. EPR and ELDOR studies on spin relaxation in perdeuterated 2,2,6,6-tetramethyl-4-piperidone-N-oxyl in liquid solutions: The slowly relaxing local structure mechanism. J Phys Chem. 1984; 88:2275–2284.
32. Freed, JH. Theory of Multiple Resonance and ESR Saturation in Liquids and Related Media. In: Dorio, MM.; Freed, JH., editors. Multiple Electron Resonance Spectroscopy. Plenum; New York: 1979. p. 100

33. Banci, L.; Bertini, I.; Luchinat, C. Electron Relaxation in Dilute Systems. Nuclear and Electron Relaxation, VCH; Weinheim: 1991. p. 71-90.
34. Eastman MP, Bruno GV, Freed JH. ESR Studies of Heisenberg Spin Exchange III An ELDOR Study. J Chem Phys. 1970; 52:321–327.
35. Bowman MK, Michalski TJ, Peric M, Halpern HJ. Fourier Transform EPR and Low Frequency EPR studies of nitroxide radicals. Pure & Appl Chem. 1990; 62:271–274.
36. Halpern HJ, Peric M, Yu C, Bales BL. Rapid quantitation of parameters from inhomogeneously broadened EPR spectra. J Magn Reson A. 1993; 103:13–22.
37. More KM, Eaton GR, Eaton SS. Determination of T_1 and T_2 by simulation of EPR power saturation curves and saturated spectra. Application to spin-labeled iron porphyrins. J Magn Reson. 1984; 60:54–65.
38. Burks SR, Makowsky MA, Yaffe ZA, Hoggle C, Tsai P, Muralidharan S, Bowman MK, Kao JPY, Rosen GM. The Effect of Structure on Nitroxide EPR Spectral Linewidth. J Org Chem. 2010; 75:4737–4741. [PubMed: 20540511]
39. Jones LL, Schwartz RN. An electron paramagnetic resonance study of rotational and translational motion in solution. Mol Phys. 1981; 43:527–555.
40. Kooser RG, Volland WV, Freed JH. E.S.R. relaxation studies on orbitally degenerate free radicals. I. Benzene anion and tropenyl. J Chem Phys. 1969; 50:5243–5257.
41. Mossoba MM, Makino K, Riesz P, Perkins RC. Long-range proton hyperfine coupling in alicyclic nitroxide radicals by resolution-enhanced electron paramagnetic resonance. J Phys Chem. 1984; 88:4717–4723.
42. Sastry VSS, Polimeno A, Crepeau RH, Freed JH. Studies of spin relaxation and molecular dynamics in liquid crystals by two-dimensional Fourier transform electron spin resonance. II. Perdeuterated-tempone in butoxy benzylidene octylaniline and dynamic cage effects. J Chem Phys. 1996; 105:5773–5791.
43. Freed, JH. Theory of slow tumbling ESR spectra of nitroxides. In: Berliner, LJ., editor. Spin Labeling: Theory and Applications. Academic Press; New York: 1976. p. 53-132.
44. Eastman MP, Bruno GV, Freed JH. ESR Studies of Heisenberg Spin Exchange. II. Effects of Radical Charge and Size. J Chem Phys. 1970; 52:2511–2522.
45. Yager TD, Eaton GR, Eaton SS. $[Cr(oxalate)_3]^{3-}$ as a broadening agent in nitroxyl spin probe studies. J Chem Soc Chem Comm. 1978:944–5.
46. Dalal DP, Damoder R, Benner C, Eaton GR, Eaton SS. Metal-nitroxyl interactions. 44. Collision interactions between transition metal complexes and nitroxyl radicals in aqueous solution. J Magn Reson. 1985; 63:125–32.
47. Epel B, Haney CR, Hleihel D, Wardrip C, Barth ED, Halpern HJ. Electron paramagnetic resonance oxygen imaging of a rabbit tumor using localized spin probe delivery. Med Phys. 2010; 37:2553–2559. [PubMed: 20632567]
48. Williams BB, Halpern HJ. In vivo EPR imaging. Biol Magn Reson. 2005; 23:283–319.
49. Tseitlin M, Dhami A, Quine RW, Rinard GA, Eaton SS, Eaton GR. Electron Spin T_2 of a Nitroxyl Radical at 250 MHz Measured by Rapid Scan EPR. Appl Magn Reson. 2006; 30:651–656.

- Six nitroxides were studied at X-band in the rapid tumbling regime.
- T_1 and T_2 were measured by pulse methods and CW linewidths were simulated.
- T_1 and T_2 are longer for ^{15}N than for ^{14}N and are dependent on m_I.
- Relaxation times at low frequency are predicted to be similar to values at X-band.

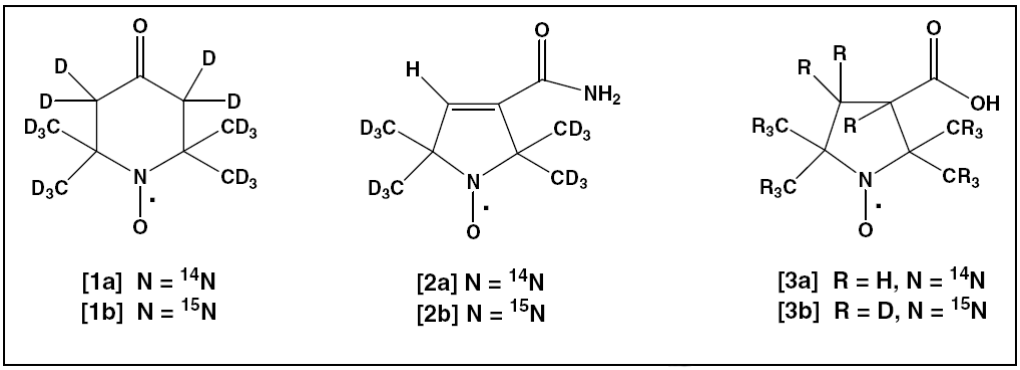

Fig. 1.

Structures of nitroxides studied. The designations **1, 2**, or **3** are used when referring to either nitrogen nuclear isotope. Tempone and mHCTPO are commonly used designations for **1** and **2**, respectively.

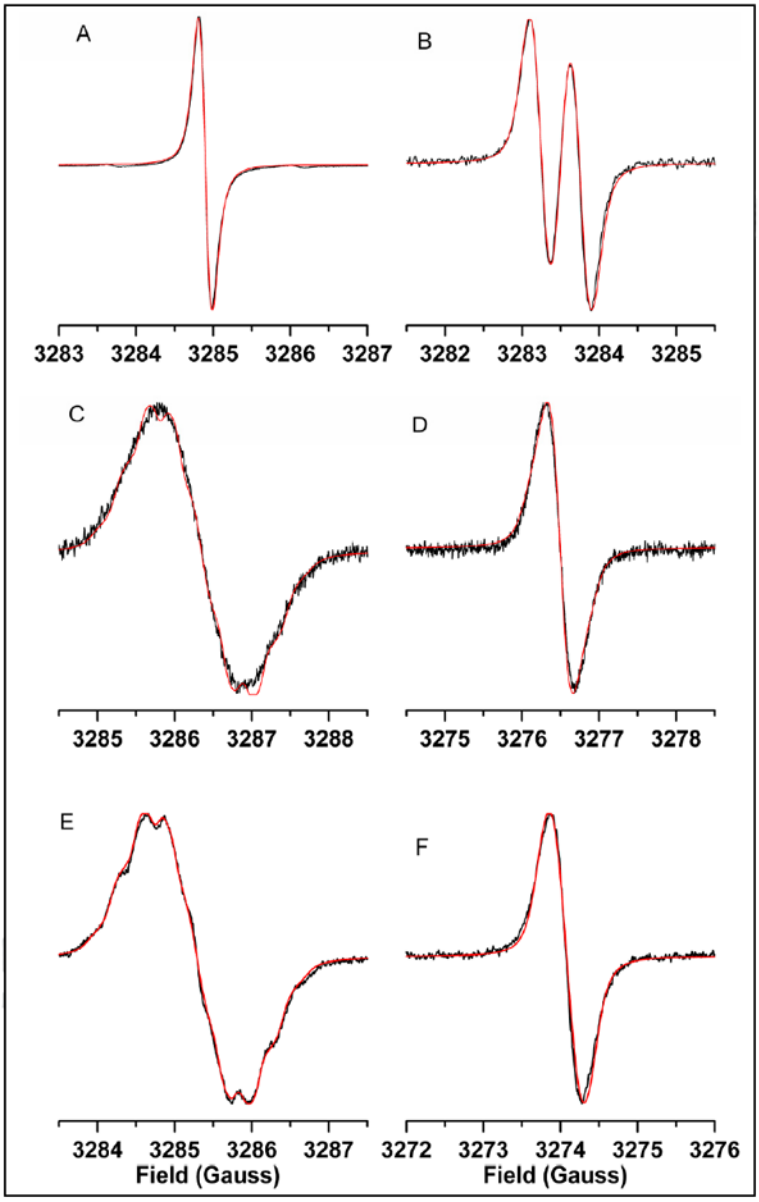

Fig. 2.

CW lineshapes in the absence of oxygen for center-field lines of (A) **1a** in water, (B) **2a** in water, (C) **3a** in water, (D) low-field line of **3b** in water (E) center-field line of **3a** in toluene, and (F) low-field line of **3b** in toluene. For each of the plots the x axis spans 4 G and the y axis scale is arbitrary. Simulations (red lines) using the hydrogen/deuterium hyperfine couplings listed in Table 6 and the spin packet widths listed in Table 1 overlay the experimental spectra.

Table 1

Relaxation Times, Spin Packet Widths and Overall Line Widths in H_2O at 0.25 mM[a]

nitroxide	T_1 (μs)[b]	T_2 (μs)[c]	ΔB_{sp} (G)[d]	ΔB_{pp} (G)
1a	0.59	0.56	0.12	0.16
2a	0.67	0.53	0.12	0.51[e]
3a	0.72	0.57	0.11	1.1
1b	0.81	0.64	0.10	0.16
2b	0.86	0.60	0.11	0.51
3b	1.0	0.75	0.087	0.40

[a] Center-field line for ^{14}N and low-field line for ^{15}N in deoxygenated water at 20-22°C.

[b] Uncertainties are about ± 0.03 μs.

[c] Uncertainties are about ± 0.02 μs.

[d] Calculated from T_2 using Eq. (1).

[e] The partially-resolved doublet splitting is 0.51 G with ΔB_{pp} for each component of 0.26 G.

Table 2

Average T_1[a] (μs) at 0.030 mM in H_2O and Comparison with Calculations[b]

nitroxide	Exp.[a]	Calc. with (Eq. 2)	Calc. with Eq. (2), (3), (4).	Calc. with Eq. (2), (3), (5)[c]
1a	0.75	1.3	0.72	0.75
2a	0.84	1.9	0.80	0.83
3a	0.87	2.7	0.91	0.94
1b	0.91	1.3	0.81	0.84
2b	1.0	1.9	0.94	0.97
3b	1.05	1.7	1.1	1.1

[a] Experimental T_1, average of values obtained for low-field, center-field, and high-field lines.

[b] Calculations use τ = 9, 13, and 19 ps for **1, 2**, and **3**, respectively.

[c] $\beta = 0.90$

Table 3

[a] Ratios of T_1 for nitrogen hyperfine lines

Nitroxide	T_1^{LF}/T_1^{CF}	T_1^{CF}/T_1^{HF}	T_1^{LF}/T_1^{HF}	Replicates
1a	1.11 ± 0.02	1.10 ± 0.04	1.22 ± 0.04	33
2a	1.12 ± 0.03	1.08 ± 0.07	1.22 ± 0.07	10
3a	1.16 ± 0.02	1.09 ± 0.04	1.26 ± 0.06	12
1b			1.18 ± 0.03	12
2b			1.19 ± 0.05	11
3b			1.23 ± 0.02	10

[a] LF, CF, and HF designate the low-field, center-field, and high-field lines. For ^{14}N m_I = +1, 0, and -1 for the low-field, center-field, and high-field lines. For ^{15}N m_I = 0.5 and -0.5 for the low-field and high-field lines.

Table 4

[a] Differences between relaxation rates[b] for nitrogen hyperfine lines

Nitroxide	$1/T_1^{LF} - 1/T_1^{HF}$ experimental[c]	$1/T_1^{LF} - 1/T_1^{HF}$ Calc, Eq. 7[d]
1a	-0.32 ± 0.06	-0.26
2a	-0.26 ± 0.08	-0.30
3a	-0.29 ± 0.06	-0.30
1b	-0.21 ± 0.03	-0.18
2b	-0.19 ± 0.04	-0.21
3b	-0.21 ± 0.01	-0.22

[a] Notation and number of replicates are the same as in Table 3.

[b] Units are 10^6 s^{-1}

[c] Proportional to $\Delta m_I = 2$ for ^{14}N, $\Delta m_I = 1$ for ^{15}N

[d] $c_1' = -0.32$

Table 5

Concentration Dependence of Spin Packet Line Widths and Widths in H_2O at Infinite Dilution

nitroxide	intercept ΔB_{sp} (G)[a,b]	slope, mG/mM[a]
1a	0.09	100
2a	0.09	160
3a	0.09	80
1b	0.07	120
2b	0.07	170
3b	0.07	80

[a] Rounded to nearest 10 mG, which is the estimated uncertainty.

[b] Calculated from T_2 measured by spin echo.

Table 6

Nitrogen and hydrogen/deuterium coupling constants (G) in H_2O[a,b]

	1a	2a	3a	3b
N	16.1	16.1	16.4	22.9
methyl	0.018 (12D)	0.027 (12D)	0.32 (3H)	0.049 (3D)
			0.28 (3H)	0.043 (3D)
			0.05 (3H)	0.008 (3D)
			0.04 (3H)	0.006 (3D)
ring hydrogens	0.0031 (4D)	0.51 G (1H)	0.54 (1H)	0.54 (1H)/0.083 (1D) 1:3
			0.14 (1 H)	0.021 (1D)
			0.12 (1H)	0.018 (1D)

[a] Coupling constants for **1b** and for **2b** are the same as for the corresponding ^{14}N analogs except for scaling of the nitrogen hyperfine coupling.

[b] Hyperfine coupling constants are in good agreement with literature values for **1a** [12], **2a** [12,13], nitroxides similar to **3** [14].